ARL-TR-7507 ● OCT 2015

US Army Research Laboratory

Non-Contact Circuit for Real-Time Electric and Magnetic Field Measurements

by Sean M Heintzelman

Approved for public release; distribution unlimited.

NOTICES

Disclaimers

The findings in this report are not to be construed as an official Department of the Army position unless so designated by other authorized documents.

Citation of manufacturer's or trade names does not constitute an official endorsement or approval of the use thereof.

Destroy this report when it is no longer needed. Do not return it to the originator.

ARL-TR-7507 ● OCT 2015

US Army Research Laboratory

Non-Contact Circuit for Real-Time Electric and Magnetic Field Measurements

by Sean M Heintzelman
Sensors and Electron Devices Directorate, ARL

Approved for public release; distribution unlimited.

REPORT DOCUMENTATION PAGE

Form Approved
OMB No. 0704-0188

Public reporting burden for this collection of information is estimated to average 1 hour per response, including the time for reviewing instructions, searching existing data sources, gathering and maintaining the data needed, and completing and reviewing the collection information. Send comments regarding this burden estimate or any other aspect of this collection of information, including suggestions for reducing the burden, to Department of Defense, Washington Headquarters Services, Directorate for Information Operations and Reports (0704-0188), 1215 Jefferson Davis Highway, Suite 1204, Arlington, VA 22202-4302. Respondents should be aware that notwithstanding any other provision of law, no person shall be subject to any penalty for failing to comply with a collection of information if it does not display a currently valid OMB control number.
PLEASE DO NOT RETURN YOUR FORM TO THE ABOVE ADDRESS.

1. REPORT DATE *(DD-MM-YYYY)*	2. REPORT TYPE	3. DATES COVERED (From - To)
October 2015	Final	3/2015–8/2015

4. TITLE AND SUBTITLE
Non-Contact Circuit for Real-Time Electric and Magnetic Field Measurements

5a. CONTRACT NUMBER

5b. GRANT NUMBER

5c. PROGRAM ELEMENT NUMBER

6. AUTHOR(S)
Sean M Heintzelman

5d. PROJECT NUMBER

5e. TASK NUMBER

5f. WORK UNIT NUMBER

7. PERFORMING ORGANIZATION NAME(S) AND ADDRESS(ES)
US Army Research Laboratory
ATTN: RDRL-SES-P
2800 Powder Mill Road
Adelphi, MD 20783-1138

8. PERFORMING ORGANIZATION REPORT NUMBER
ARL-TR-7507

9. SPONSORING/MONITORING AGENCY NAME(S) AND ADDRESS(ES)

10. SPONSOR/MONITOR'S ACRONYM(S)

11. SPONSOR/MONITOR'S REPORT NUMBER(S)

12. DISTRIBUTION/AVAILABILITY STATEMENT
Approved for public release; distribution unlimited.

13. SUPPLEMENTARY NOTES

14. ABSTRACT
This report describes the US Army Research Laboratory (ARL) multimodal D-dot (MD-dot) sensor, a 1.25 inch x 2 inch integrated circuit that can stand alone or be attached to an energized conductor to measure both electric and magnetic fields simultaneously. The MD-dot circuit has programmable 0 to 80 dB output gain and 0–3.3 V DC offset to maximize dynamic range. Furthermore, active output control allows us to vary the signals for compatibility with most data acquisition (DAQ) input requirements; however, it is designed to work best with the ARL Real-Time Electric and Magnetic Integrated Sensor (ARTEMIS) smart sensing node. The gain and offset are programmed with 1Wire communication protocol, but are also compatible with serial peripheral interface (SPI) and universal asynchronous receiver-transmitter (UART) for increased programming flexibility. The gain and offset accuracy for the MD-dot is measured to allow real-time calculation of electric and magnetic fields. An ARL-designed electric-field cage is used to generate electric fields and characterize the sensor's frequency response, noise spectral density, and dynamic range.

15. SUBJECT TERMS
electric field, magnetic field, 1Wire, low-power microcontroller

16. SECURITY CLASSIFICATION OF:			17. LIMITATION OF ABSTRACT	18. NUMBER OF PAGES	19a. NAME OF RESPONSIBLE PERSON
a. REPORT	b. ABSTRACT	c. THIS PAGE			Sean M Heintzelman
Unclassified	Unclassified	Unclassified	UU	24	19b. TELEPHONE NUMBER (Include area code) 301-394-1844

Standard Form 298 (Rev. 8/98)
Prescribed by ANSI Std. Z39.18

Contents

List of Figures

Acknowledgments

I would like to acknowledge Simon Ghionea and David Bartlett for design and hardware support, and Dave Hull for work on the original version of this report.

INTENTIONALLY LEFT BLANK.

1. Introduction

An energized electric power cable generates low-frequency electric and magnetic fields that are related to the voltages and currents. Especially at wavelengths $\lambda >> d$, where d is the distance away from an energized conductor and λ is the signal wavelength, we can extract electrical information with quasi-static near-field electric and magnetic field theory and the Principle of Superposition.

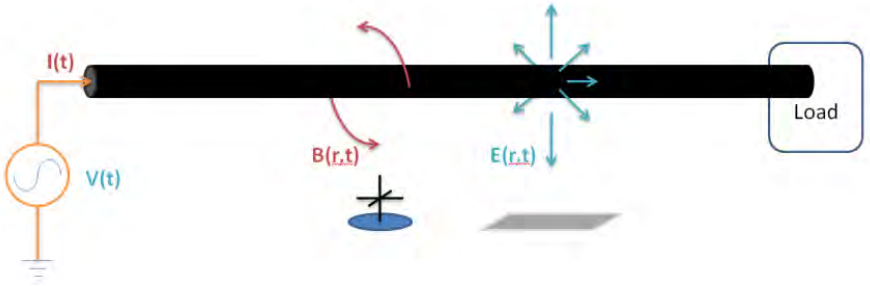

Fig. 1 Standard experimental setup for measuring magnetic and electric fields emitted by and energized cable with an attached load. Blue circle represents a B-field sensor, gray plate represents an E-field (charge) sensor.

Coulomb's and Biot-Savart Laws, respectively, relate the electric and magnetic fields to the voltage V and current I on a single straight energized wire:

$$\vec{E} = \frac{\rho(V)}{\varepsilon_0 2\pi d}\,\hat{a}_r \tag{1}$$

$$\vec{B} = \frac{\mu_0 I}{2\pi d}\hat{a}_\varphi \tag{2}$$

where μ_0 and ε_0 are magnetic permeability and electric permittivity constants, ρ is the surface charge density on the wire, and a_φ and a_r are vectors pointing in the direction of the field in cylindrical coordinates. Superposition principles are used with Coulomb and Biot-Savart Laws in multi-wire configurations (i.e., 3-phase power cables). The boundary element method or electromagnetic models are typically used to solve for $\rho(V)$, which changes minimally along the length of the wire at quasi-static frequencies.[1]

There are many commercial-off-the-shelf (COTS) and Government-off-the-shelf (GOTS) sensors for making non-contact electric- and magnetic-field measurements. The electric-field (E-field) sensing team at ARL has previously characterized several E-field sensors, including SAIC Steered-Electron Electric-Field (SEEF) sensor, Srico optical sensor, Plessey EPIC sensors, QUASAR non-contact capacitive "dime" sensors, QFS 3-axis low-frequency (LF) E-field sensors, and the University North Carolina Charlotte (UNCC) custom E-field sensor.[2] These

sensors have produced good results,[3] but do not include real-time programming abilities for signal conditioning. Furthermore there are no COTS or GOTS 1Wire compatible electric- and magnetic-field sensors. Therefore, there is a need for integrated multimodal (electric- and magnetic-field) programmable sensors that are specifically designed for sensing the fields near energized cables. ARL's multimodal D-dot (MD-dot) sensor addresses these needs, and additionally has "smart" features that adjust integrated circuits (ICs) on the sensor during start-up based upon the electrical characteristics of the attached cable.

2. Methods and Procedures

The circuit's primary design consists of a microcontroller, 8-channel digital-to-analog converter (DAC), variable gain chips, differential operational amplifiers, and E-field and B-field sensors. These components work together to form an interface that allows both onboard and external programming of the sensor, all while measuring electric and magnetic fields. Their connections are summarized in Fig. 2.

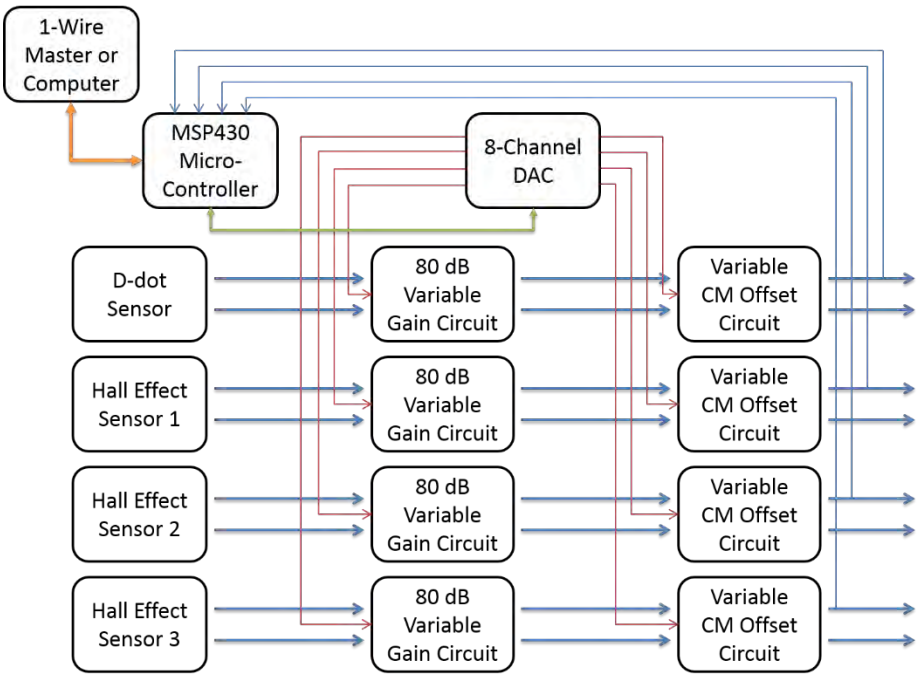

Fig. 2 Block diagram showing the high-level architecture of the MD-dot

The circuit works in the following manner to set its own gain voltage and offset voltage, resulting in optimized output signal characteristics:

1. Microcontroller reads ferroelectric random-access memory (FRAM) for current DAC output on 1 of its 8 channels.

2. Microcontroller changes digital value for 1 of 8 DAC channels by serial peripheral interface (SPI) protocol (green).
3. DAC sets corresponding analog output voltage to desired variable circuit input (red).
4. Variable gain and/or variable offset stage outputs reflect changes (thick blue).
5. Output signal is measured by microcontroller's analog-to-digital converters (ADCs) (thin blue).
6. Microcontroller increases or decreases (repeat 1–5) DAC setting, or keeps DAC setting based on ADC measurement and stores in FRAM

2.1 Sensors

The magnetic field is measured by MLX91205 Hall effect sensors.[4] We use three 1-dimensional Hall effect sensors arranged in a line across an energized power cable to measure the magnetic field at 3 spatially diverse locations. These sensors can give an accurate measurement of a +/–10 mT magnetic field in the azimuthal direction. The MLX91205 output voltage is linear with magnetic-field strength up to a maximum chip output of 50-mV amplitude; therefore, we can compute the magnetic sensitivity Ω for the sensor:

$$\Omega = \frac{V_{out}}{B} = 5\frac{V}{T} \tag{3}$$

The electric field is measured by a small D-dot sensor. The principle of operation for D-dot sensors is charge induction between a grounded electrode and an energized cable; the operational details of operation can be found elsewhere.[5] The sensing electrode for the MD-dot is the area inside the yellow outlined region of Fig. 3. The copper-outlined region, along with a mimicked layer directly underneath the layer shown, act as a shield driven at 1.65 V. The shield results in minimal sensing electrode capacitance with field sources in unwanted directions (not parallel to and below the sensing electrode), therefore less noise and greater directionality in our measurement.

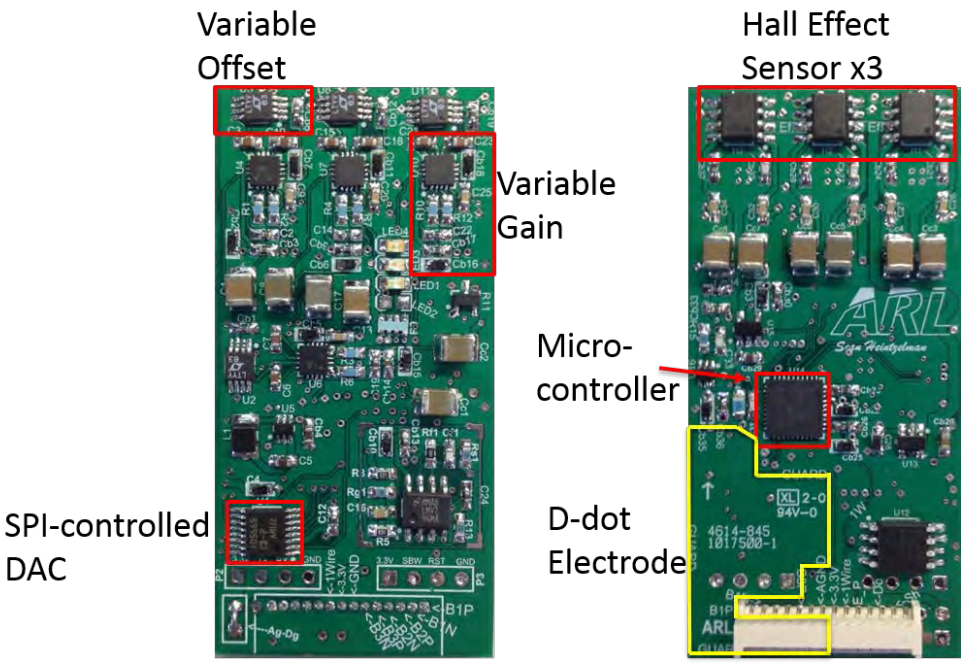

Fig. 3 Front (left) and back (right) sides of an MD-dot circuit board. Our D-dot sensing electrode is highlighted in yellow and is made out of an isolated piece of copper on the PCB.

The area of the D-dot electrode is ~243 mm^2. The output current from the D-dot sensing electrode connected to a differentiator given by

$$i_{DDOT} = \frac{dQ}{dt} = \varepsilon A_{eff} \frac{dE_z}{dt} = \omega \varepsilon A_{eff} E_{z0} \sin(\omega t + \varphi) \tag{4}$$

where ε is the free space permittivity, ω is frequency, φ is the E-field phase, E_{z0} is the amplitude of the electric field, and A_{eff} is the effective area of the D-dot plate i.e., 243 mm times an enhancement factor. This enhancement factor approximately equals 1 in our design; however, enhancement factors have been demonstrated as high as 8.[6] The D-dot current i is fed into a transimpedance amplifier with a gain of $1 \frac{V}{mA}$. The final output of the D-dot sensors is

$$v_{DDOT} = 1000 i_{DDOT} = \beta \omega E_{z0} \sin(\omega t + \varphi) \tag{5}$$

where we have used i_{DDOT} from Eq. 4 and introduced a constant β equal to $1000 \varepsilon A_{eff}$, which represents a frequency-independent transducer gain. We now have a relationship constant for reverse-calculating the electric field E (neglecting phase differences):

$$\beta \omega = \frac{v_{DDOT}}{E} = (2.15 \cdot 10^{-12}) \omega \frac{V}{s \cdot V/m} \tag{6}$$

where β is presented in physically-meaningful units.

2.2 Variable Gain and Offset Stage

The differential output currents of all MLX91205 Hall effect sensors and the D-dot sensor are connected to a variable gain AD8338 chip. This chip can change gain magnitude across an 80-dB (1–10000 times) range depending on a supplied gain voltage V_g. The AD8338 chip and associated resistors and capacitors make up the Fig. 2's "variable gain circuit."

The DC offset of the output signal is slightly dependent on both the input DC offset and V_g, so we can ensure a DC offset at 1.65 V with a LTC1992-2 differential operational amplifier immediately following the AD8338 chip. The LTC1992-2 common-mode voltage (V_{CM}) pin(s) connected are different channels on an AD5668 8-channel 16-bit DAC.[7] We can therefore vary the voltage on each of V_{CM} pins, thereby the DC offset of LTC1992-2 output. The LTC1992-2 and associated capacitors make Fig. 2's "variable offset circuit."

2.3 Embedded System Integration

The Texas Instruments (TI) MSP430FR5739 microcontroller acts as the master for SPI and simulated 1Wire devices on the MD-dot, but as a slave 1Wire device for the ARL Real-Time Electric and Magnetic Integrated Sensor (ARTEMIS). This microcontroller was programmed with Code Composer Studio (CCS) 6.0.0 software to run at 16 MHz for minimal power consumption while still falling within 1Wire protocol timing restrictions. The MSP430 pins are designated for 5 primary purposes:

1) SPI communication: 3 pins for serial clock (SLCK), master output to salve input (MOSI) (which we use to program each output DAC channel for variable gain and offset voltages), and master input to slave output (MISO). These lines connect directly to AD5668 chip to control the analog output voltage on each of its 8 output channels.

2) Universal asynchronous receiver/transmitter (UART) communication: 2 pins for communication with UART devices, available as jumpers on the board to allow external interfacing. These pins are not used for normal operation of the integrated D-dot, but can be used for onsite programming when a 1Wire master is not available.

3) 1Wire communication: 3 pins are designed for compatibility with 1Wire communication protocol. One pin is used for the 1Wire communication line, and 2 other pins are for "test" and "reset." These 3 pins are connected to jumpers for sensor software updates.

4) Self-Calibration: 4 pins (FBADCx Fig. 4) are designated as inputs to 10-bit ADCs with our 4 differential output signals as inputs. The MSP430 uses these pins to measure the output signal and adjust the variable gains and offsets, specifically so the output signal occupies a desired percentage of any DAQ's input range.

5) Experimental Error Detection: 4 pins are connected to a light-emitting diode (LED) array. Depending on the unique experimental or user-driven demands, these are programmed to light-up to indicate specific errors at start-up or during a long-term test.

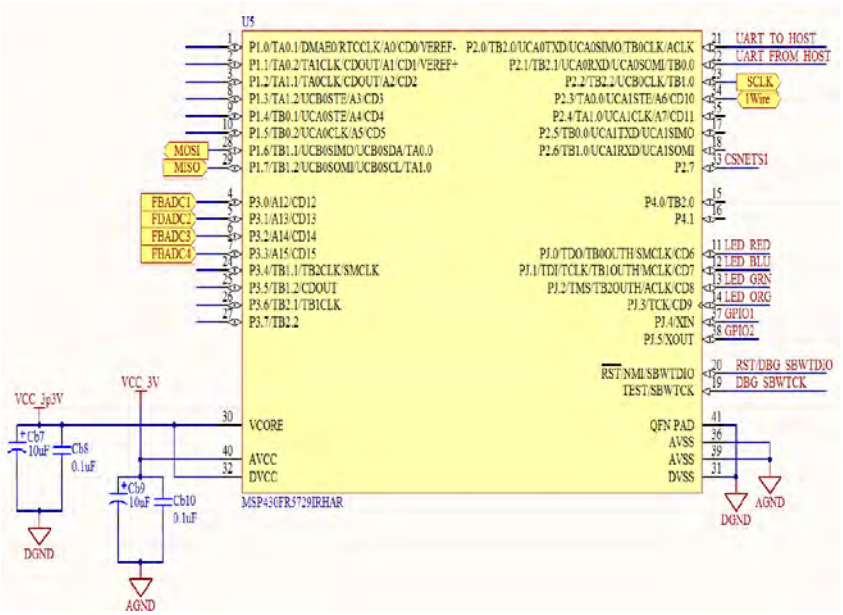

Fig. 4 Altium Designer™ schematic showing the pin connections of our MSP430 microcontroller

2.4 1Wire Interfacing

The author of this paper has successfully developed 1Wire Code Composer Studio (CCS) software compatible with the TI's MSP430 microcontroller line and 1Wire protocol.[8] The ability to read, write, and communicate with arbitrary 1Wire masters was established. The software has capabilities to emulate the DS2408 and DS24B33 (1Wire 8-channel switch and 1Wire electrically erasable programmable read-only memory [EEPROM]) slave devices produced by MAXIM, both of which are required with ARTEMIS' specialized 1Wire protocol.

The MD-dot has been designed to be compatible with a standard 14-pin LEMO® cable to connect to analog sensors. 11 of the 14 pins are designated and currently used for 4 differential signals, power, analog ground, and 1Wire communication.

Other pins are designated for ground and D-dot electrode shielding control, however, are not used for the purposes of this report.

3. Results and Discussion

3.1 Variable Gain and Offset Characterization

In order to characterize the performance of the circuit, one must determine the input and output signal magnitudes for an array of gain voltages and offset values. This is done through the use of state-of-the-art LABVIEW and CCS programs developed in-laboratory, along with an NI9239 24-bit ADC. The software is explained at the top-level due to complexity and rigorousness.

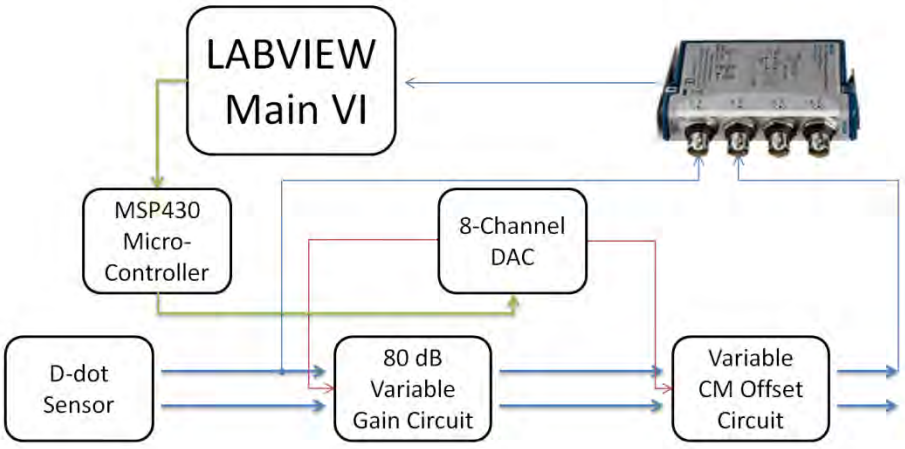

Fig. 5 Experimental setup for measuring the linearity and accuracy of variable stage components

A specialized LABVIEW VI sends 1Wire function commands to the MSP430 through a DS9490R 1Wire master device (Fig. 6). The 1Wire "function commands" step through an array of "N" variable gain or "M" offset voltages, while a NI9239 DAQ simultaneously measures the inputs and outputs of the complete variable stage. Each measurement is logged and output to a formatted Excel file. At our chosen testing frequencies (<200 Hz), the variable gain input signal is attenuated <1% due to impedances of the NI9239; this knowledge can be used for post-processing data.

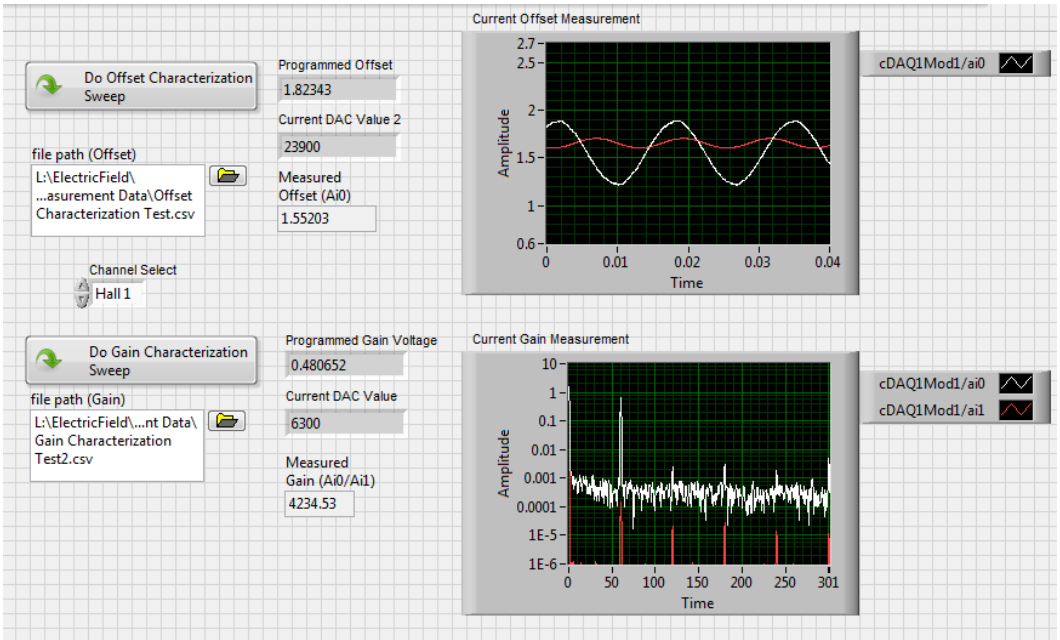

Fig. 6 Front panel of custom LABVIEW program for gain/offset characterization. Here 1 of the Hall effect sensor outputs (in dropdown box) for this measurement has been selected.

Figure 7 is a snippet of the measurement results for characterizing the MLX91205 variable gains and offsets with Nx1 and Mx1 matrices, as mentioned earlier. The data from these Excel files can be used to back-calculate the MLX91205 or D-dot sensor's output for any programmed gain or offset (variable stage is same for both sensor types), and therefore, the magnitude of the magnetic and electric fields at our sensor are given by Eqs. 3 and 6. We note that our offset voltage is noticeably lower than the programmed voltage by greater than 200 mV; this is expected when the input DC offset differs from the desired offset.

	DAC Setting	DAC Voltage	60 Hz FFT gain
2	6000	0.457764	5092.124289
3	6100	0.465393	4862.59267
4	6200	0.473022	4598.144842
5	6300	0.480652	4339.549022
6	6400	0.488281	4144.847709
7	6500	0.495911	3946.281511
8	6600	0.50354	3722.649568
9	6700	0.511169	3526.414926
10	6800	0.518799	3336.030223
11	6900	0.526428	3170.166164
12	7000	0.534058	2993.830624
13	7100	0.541687	2846.01867
14	7200	0.549316	2688.433895
15	7300	0.556946	2556.979426
16	7400	0.564575	2419.144756
17	7500	0.572205	2299.048451
18	7600	0.579834	2170.722472
19	7700	0.587463	2069.399979
20	7800	0.595093	1972.239655
21	7900	0.602722	1871.586178

	DAC Setting	Programmed Offset	Actual Offset
2	21000	1.602173	1.373248
3	21200	1.617432	1.38551
4	21400	1.63269	1.399294
5	21600	1.647949	1.409428
6	21800	1.663208	1.42343
7	22000	1.678467	1.439266
8	22200	1.693726	1.448081
9	22400	1.708984	1.459201
10	22600	1.724243	1.472795
11	22800	1.739502	1.484086
12	23000	1.754761	1.497399
13	23200	1.77002	1.511193
14	23400	1.785278	1.523542
15	23600	1.800537	1.538696
16	23800	1.815796	1.549578
17	24000	1.831055	1.565082
18	24200	1.846313	1.576122
19	24400	1.861572	1.587304
20	24600	1.876831	1.597977
21	24800	1.89209	1.613321

Fig. 7 Excel outputs generated by our LABVIEW test script to develop relationships between the DAC setting (AD5668) and circuit output. Results are only shown for 20 DAC settings to avoid redundancy.

This gain characterization allows us to correlate a volt per volt (V/V) gain with DAC values. With this information characterized, we can derive electric field magnitude of our source:

$$|E| = \frac{V_{out}}{\beta \omega G_{DAC}} \tag{7}$$

$$|B| = \frac{V_{out}}{\Omega G_{DAC}} \tag{8}$$

where G_{DAC} refers to the V/V gain value correlated to the programmed DAC value. G_{DAC} is also readable in real-time with the ARTEMIS or a generic 1Wire master.

3.2 Digital Noise

We are interested in determining our E-field sensor's susceptibility to digital noise caused by capacitive coupling with onboard communication lines, which occurs during real-time gain and offset adjustments. In order to complete this measurement, the microcontroller was programmed to write "01" indefinitely on the 1Wire line. This line is used as the reference input to a Signal Recovery DSP7270 lock-in amplifier. Using any of the 8 MD-dot's single-ended outputs with the lock-in amplifier, one can measure the digital noise on the output signals. However, I perform this test with an output line from the E-field sensor for worst-case scenario analysis: the most digital noise will appear on this line due to the

board layout (sensing electrode closest to 1Wire line) and sensor size ($A_{D\text{-}dot} > A_{LMX91205}$).

Here the digital noise is found to be 13 uV_{pk}, 80–110 dB below the typical output signal magnitude. On typical 16- and 24-bit data recorders, this results in 0–6 least significant bits of data being susceptible to corruption from digital noise.

3.3 Frequency Response

An ideal D-dot sensor would produce a linear frequency response over the region of interest, meaning the integrated sensor output will be flat for all frequencies (integration in frequency domain is performed by dividing the output by $2\pi f$). Figure 8 shows the original and integrated sensor outputs to electric fields with frequencies 10 Hz–10k Hz and magnitudes 0.357–3.571 V/m. Our sensor was set to the maximum gain value for this test, since our generated electric-field magnitudes are toward the bottom of our sensor's dynamic range.

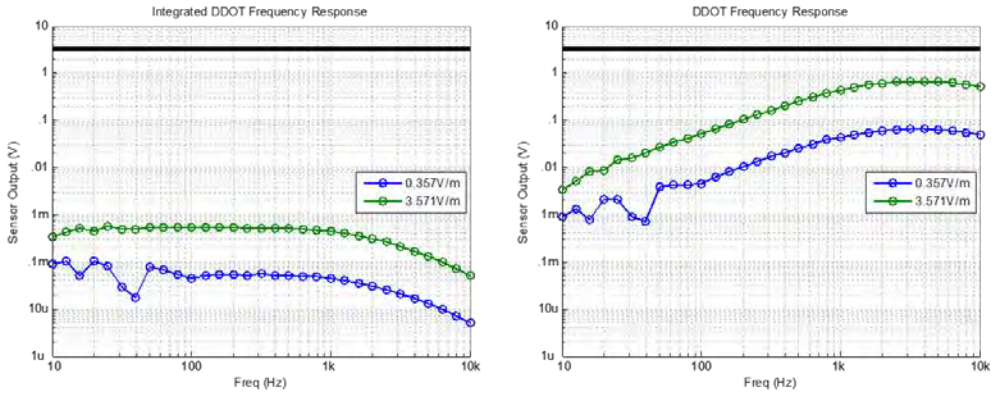

Fig. 8 Frequency response four the D-dot sensor with 80-dB on-chip gain, with additional 40-dB gain applied at the output to reduce effects of environmental noise

One can observe that the integrated response of the sensor is approximately flat for 50–800 Hz frequencies at 3.571 V/m field strength. The low sensor output at low frequencies has a signal-to-noise ratio (SNR) near 1, which distorts lower frequency measurements, and the trans-impedance amplifier's circuitry gives the roll-off beginning at 600 Hz.

Our approximate dynamic range can also be determined from our frequency response. Regardless of programmed gain voltage, the output stage of the MD-dot has a maximum amplitude of 3.3 V with 1.65 V DC offset. A 3.57-V/m field, 80-dB on-chip programmed gain, and 40-dB off-chip gain results in an output maximum of ~0.7 V as shown above. With variable gain lowered to 0 dB and off-chip gain removed, the MD-dot should be able to detect electric fields on the order

of MV/m. Putting together this information, we find the dynamic range (with 0.2-s fast Fourier transform [FFT] sampling time at 50 kS/s) is approximately 128 dB.

Although I did not have a comparable characterization system for the Hall effect sensors, the datasheet information on the MLX91205 gives a dynamic range of 66 to 96 dB for frequencies of 10 Hz and 10 kHz, respectively.[4] For magnetic-field strengths, the field-referred dynamic range is 25 μT–25 mT (10 Hz) or 79 nT–25 mT (10 kHz).

3.4 Field-Referred Noise Spectral Density

To get an idea of the minimum detectable electric field for this sensor under near-ideal conditions, a 10-s FFT was performed on the sensor with both endplates of the E-field cage grounded. The frequency response graph above is used to determine a constant value *C* to relate the E-field magnitude to the output voltage, and found to be 0.46 mV/{V/m}. By measuring the output voltage noise floor of the sensor and dividing all frequencies by *C*, a noise floor can be found in terms of E-field magnitude called the field-referred noise spectral density (FRNSD). One can also divide the voltage noise floor for this measurement system by the end-plate separation distance to find the FRNSD of our test hardware (Fig. 9, red and green lines).

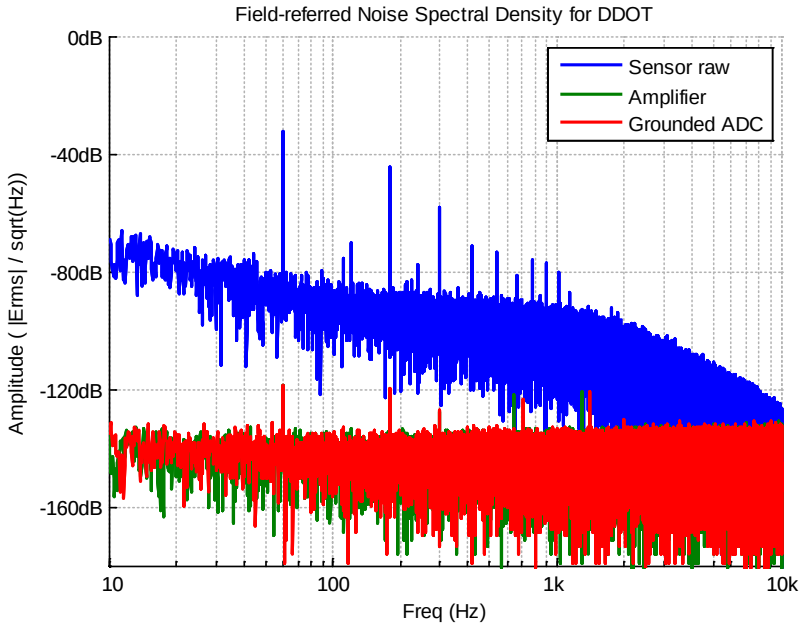

Fig. 9 Electric-field referred noise floor for our MD-dot sensor, with –60 to –85 dB field magnitude for f<800 Hz

The noise floor measured is significantly lower than in the frequency response plots; however, it can attributed to 2 main factors: a 50 times longer measurement time and additional white noise amplification by D-dot operating principle:

- For 0-mean identically and independently distributed Gaussian white noise (IIDGWN), the noise floor will decrease proportional to the square root of the measurement length, so our longer sample length will reduce noise floor by sqrt(50) or ~17 dB[9] compared to frequency response measurements
- Noise is amplified immediately after the sensing electrode proportional to its frequency: the flat-band IIDGWN is amplified by 20–80 dB in this testing bandwidth. The noise is now proportional to the square root of measurement length times the frequency, so the noise floor is reduced sqrt(500) – sqrt(500000) or 27–57 dB with the 10-s FFT length.

Our noise floor is shaped as expected for D-dot sensor, including visible effects from both 1/f noise and our 1-kHz low-pass filter. One can use our C value and integrate the FRNSD (multiply by $2\pi f$) to determine the voltage noise spectral density is primarily between 10s of μV and a single mV. These low voltages transferred in Bayonet Neill–Concelman (BNC) cables for our measurement are susceptible to noise and inhibit testing of this sensor below 1-V/m E-fields.

4. Conclusions

A small, programmable circuit capable of simultaneous electric- and magnetic-field measurements has been successfully developed. Low digital noise, over 120 dB of dynamic range, and a noise floor under ideal conditions to be less than or equal to hundreds of microvolts per meter have all been demonstrated. The sensor's dynamic and real-time programming capabilities were also confirmed by characterizing the offset and gain of the chip across a wide range of values with LABVIEW software and a 1Wire master device. To my knowledge, this is the first successful demonstration of a 1Wire compatible electric- and magnetic-field sensor. The sensor has been successfully demonstrated in continuous power-monitoring of a multi-conductor cable in a laboratory setting.[10]

5. References

1. Adelman R, Gumerov N, Duraiswami R. Accurate computation of Galerkin double surface integrals in the 3-D boundary element method IEEE Transactions on Antennas and Propagation. 2015.
2. Noras MA, Ramsey SP, Rhoades BB. Novel E-Field Sensor for Projectile Detection. Defense technical information center, October 2012.
3. Hull D, Buxton B. Detection of Electric Power Events Using Multi-Modal Sensors (U), Proceedings of the MSS meeting on Battlefield Acoustic, Seismic, Magnetic, and Electric Field Sensors. 18 August 2009.
4. Melexis. IMC-Hall Current Sensor, MLX91205 Datasheet. June. 2012
5. Vinci SJ, Hull DM. Electrostatic charge measurements and characterization of in-flight RPGs. Proceedings of the MSS meeting on Battlefield Acoustic, Seismic, Magnetic, and Electric Field Sensors, 2004.
6. Hull DM, Vinci SJ, Ladas AP. An electrostatic Proximity Sensor for Anti-Aircraft Projectile Fuzing. ARL Draft. October 2001.
7. Analog Devices. Octal 16-bit SPI Voltage Output dense DAC with 5ppm/°C On-Chip Reference, AD5668 Datasheet. 2014
8. MAXIM 1Wire Tutorial [access 2015]. http://www.maximintegrated.com/en/app-notes/index.mvp/id/74.
9. Cerna M, Harvey A. The Fundamentals of FFT-Based Signal Analysis and Measurement. Application Note 041. July, 2000.
10. Parks BS, Hull DM, Adelman RN. Three-Phase Power Monitoring in Multi-Conductor Power Cables. Adelphi (MD): Army Research Laboratory (US); 2015 Sep. Report No.: ARL TR-2437

List of Symbols, Abbreviations, and Acronyms

ADC	analog-to-digital converter
ARL	US Army Research Laboratory
ARTEMIS	ARL Real-Time Electric and Magnetic Integrated Sensor
B-field	magnetic field
BNC	Bayonet Neill–Concelman
CCS	Code Composer Studio
COTS	commercial-off-the-shelf
DAC	digital-to-analog converter
DAQ	data acquisition
EEPROM	electrically erasable programmable read-only memory
E-field	electric field
FFT	fast Fourier transform
FRAM	ferroelectric random access memory
FRNSD	field-referred noise spectral density
GOTS	Government-off-the-shelf
IC	integrated circuit
IIDGWN	independently distributed Gaussian white noise
LED	light-emitting diode
LF	low-frequency
MISO	master input to slave output
MOSI	master output to salve input
PCB	printed circuit board
q , Q	electric charge
SEEF	Steered-Electron Electric-Field
SLCK	serial clock
SNR	signal-to-noise ratio

SPI	serial peripheral interface
TI	Texas Instruments
UART	universal asynchronous receiver/transmitter
UNCC	University North Carolina Charlotte
VI	Visual Instrument
μ	micro-, meaning 10^{-6} times whatever terms proceeds it

1 DEFENSE TECH INFO CTR
(PDF) DTIC OCA

2 US ARMY RSRCH LAB
(PDF) IMAL HRA MAIL & RECORDS MGMT
RDRL CIO LL TECHL LIB

1 GOVT PRINTG OFC
(PDF) A MALHOTRA

1 ARMY PM UAS
(PDF) L SHELTON

1 US ARMY RSRCH LAB
(PDF) RDRL SES P
S HEINTZELMAN